scientific reports

Check for updates

OPEN

The effects of cell displacement on DNA damages in targeted radiation therapy using Geant4-DNA

Ali Azizi Ganjgah & Payvand Taherparvar✉

Charged particle radiation can, directly and indirectly, affect cells by breaking DNA strands. This effect includes DNA single-strand breaks (SSB) and DNA double-strand breaks (DSB), which may cause cell death and mitotic failure. Thus, using short-range charged particles such as Auger electrons (AEs) not only leads to the destruction of the target cell but also prevents the nearby healthy cells from exposing to ionizing radiation. In this study, two spherical cells (C and C_2) and their cell nucleus, both made of liquid water, were modeled. An atomic DNA model constructed in the Geant4-DNA Monte Carlo (MC) simulation toolkit was placed inside the nucleus of the C and C_2 cells. The number of direct and indirect SSB, DSB, and hybrid DSB (HDSB), caused by some of the most widely-used Auger electron-emitting (AEE) radionuclides, including ^{99m}Tc, ^{111}In, ^{123}I, ^{125}I, and ^{201}Tl, distributed within different compartments of the C cell, was calculated in the C and C_2 cells, considering the distance between the surface of the two cells ranges from 0 to 5 µm. The present work aimed to investigate the biological effects of AEE radionuclides and their potential for cancer treatment through targeted radiation therapy. The results indicate the impact of ^{201}Tl > ^{125}I > ^{123}I > ^{111}In > ^{99m}Tc on DNA damage when the target is C (first spherical cell). On the other hand, for C_2 at distances of 0 to 5 µm, the impact of ^{99m}Tc > ^{123}I > ^{111}In > ^{201}Tl > ^{125}I on DNA damage is observed.

Keywords Monte Carlo study, DNA damage, SSB, DSB, HDSB, Auger electron

Targeted radionuclide therapy (TRT), also known as molecular radiotherapy, is an innovative approach to radiation therapy. TRT uses beta-emitting and alpha-emitting radionuclides to specifically affect target cells by disrupting the cell cycle and specific signaling pathways, resulting in tumor regression while minimizing damage to surrounding tissues[1]. In this technique, Auger electron-emitting (AEE) radionuclides are interesting tools for the selective administration of the optimal dosage to the tumor area while sparing the non-affected tissues[2]. The energy range of Auger electrons (AEs) spans from several eV to keV, with travel distances of only a few nanometers in the biological tissues, which potentially leads to a highly localized energy deposition[2–4]. AEE radionuclides can be attached to a targeting ligand through the use of molecular imaging agents or nanoparticles[5]. However, due to the significant linear energy transfer (LET) coupled with a short effective range, AEs are required to be brought close to the cell targets. While traditional studies of ionizing radiation effects focus primarily on nuclear DNA as the main target for inducing cytotoxicity, emerging evidence highlights that other cellular sites, notably the cell membrane, can also be highly sensitive to ionizing radiation, particularly AEs. The cell membrane is a critical target for ionizing radiation, often exhibiting greater sensitivity to AE-induced damage than the cytoplasm. AEs can contribute to the elimination of cancer cells by inducing cytotoxicity through mechanisms such as bystander or cross-dose effects. Although radiation does not directly disrupt cellular membranes, the high LET of AEs can result in significant biological damage within targeted cells, ultimately leading to cell death. This heightened sensitivity is due to intense, localized energy deposition within the membrane, which triggers signaling pathways that regulate apoptosis and cell survival. Emphasizing this point before focusing solely on the nucleus acknowledges that significant cytotoxicity can arise from targeting the membrane, not just from nuclear DNA damage. Some common AEE radionuclides used in TRT are ^{99m}Tc, ^{111}In, ^{123}I, ^{125}I, and ^{201}Tl[6–11]. Optimizing the effectiveness of the radiation therapy techniques requires an understanding mechanisms of radiation interactions with cellular systems and the subsequent biophysical implications for biological targets. DNA molecule is regarded as the most critical target for inducing radiation-mediated cytotoxicity. It has been proven that the probability of fatality escalates with the extent of unrepaired DNA impairment[12,13]. The energy deposition of the AEs can lead to some biological effects and damage to the DNA molecules through direct, deposition of energy directly onto DNA strands, and indirect, interaction with water molecules to produce

Faculty of Science, Department of Physics, University of Guilan, Namjoo Avenue, P.O. Box 41635–1914, Rasht 4193833697, Iran. ✉email: p.taherparvar@guilan.ac.ir; p.taherparvar@gmail.com

reactive species mechanisms. DNA damage can typically classify into two primary types: SSB and DSB. Although cellular repair mechanisms can repair the majority of SSBs, DSBs present significant challenges in the repair process and frequently culminate in cellular apoptosis. Hence, the DNA situated in the cell nucleus is regarded as the principal target of the effects of radiation, commonly referred to as "targeted effects"[14,15]. The study of radiation damage at the molecular scale has garnered much attention in recent years, particularly focusing on the constituents of the cell. Among these constituents, DNA molecules are considered the most vital due to their role as carriers of genetic information. Understanding the DNA damage processes is essential for accurately uncovering the biological foundations of radiation sensitivity. This understanding serves as a crucial fundamental factor in assessing the influence of radiation and ionizing therapies. Molecular-scale interactions are complicated and cannot be easily investigated through standard analytical techniques. Today, advanced radiotherapy techniques necessitate the use of theoretical analysis and experimental methods to determine radiation track structure at the nanoscale and assess radiation effects on DNA molecules at the cellular and subcellular levels[4,16–19]. Since all effects related to the radiation-induced damage in the cell scale have not yet been thoroughly assayed by experimental procedures, performing the simulation techniques is helpful to gain more knowledge of ionizing radiation effects at the cellular and subcellular levels. Consequently, numerous studies employing Monte Carlo simulations (MCS) have served as the gold standard for the evaluation of radiation measurement applications[20]. Today, with the progress made in the field of MC technique, the radiation transport and interactions as well as the distribution of its energy deposition at the subnuclear level or further at the scale of DNA molecules, can be calculated elaborately. It makes more accurate predictions of the biological effects of radiation on healthy cells by simulating complex physical and chemical interactions as well as radiation-induced DNA damage. In this way, some MCS codes are designed for accurately predict of DNA damage. These MC codes can be classified into two categories: Condensed-History (CH) and Track-Structure (TS)[21,22]. In CH codes, such as MCNP[23,24] and Penelope[25] multiple interactions are considered as one Step which leads to simulating fewer secondary particles and results in faster computation. However, these codes do not explicitly model interactions at the nanometer scale and are suitable to simulate overall macroscopic dose deposition. On the other hand, TS codes like Geant4-DNA[26,27], PARTRAC[28], Penelope, CPA100[29], and MOCA8[30] simulate step-by-step interactions at the molecular scale. They considered total and differential interaction cross-sections for particle processes with matter. Nowadays, the Geant4-DNA toolkit is frequently utilized to calculate radiation doses at the molecular scale and for radiobiological applications. Geant4 is an open-source and free MC toolkit that accurately simulates particle transport in matter such as medical physics, hadron therapy, nuclear physics, high-energy physics, and astrophysics[27,31]. The Geant4-DNA, an extension of Geant4, is one of the evaluated and powerful TS codes specifically developed for simulating the ionizing radiation track and the electromagnetic interactions of charged particles with structures of the biological environment[32]. It contains detailed physical and chemical models to simulate radiation interactions with the geometric configurations of living tissues[33]. It provides a detailed simulation of charged particle transport in liquid water and DNA constituents at the molecular scale and allows for the simulation of both direct and indirect damage to DNA. This MCS toolkit provides high-precision tracking structure simulation across energy ranges from low (approximately eV) to high (MeV).

Although there have been some reports about discrepancies between simulation results and measurements during the implementation of MCS techniques in dosimetric evaluations in cell culture studies[34], these discrepancies can be addressed by adopting a more accurate geometric model for the biological medium. Configurations of DNA model in the MC simulations include three categories: Linear cylinder model, volumetric model, and atomic model. In the linear model, cylindrical shapes are used to model the DNA structure[35]. In the volumetric model, simple shapes are used to represent the nucleobases, sugar-phosphate backbones, and other relevant structures[36]. In the atomic model, which is also used in this research, the basic atoms that compose DNA are simulated by spheres with van der Waals radius[37,38]. It is considered as a more accurate model than others. The importance of assuming the real model as much as possible for the DNA shape is undeniable in evaluating DNA damages[39]. Several studies have been done to evaluate DNA strand breaks resulting from both physical (direct) and chemical (indirect) mechanisms induced by the AEE radioisotopes in DNA model using the Geant4-DNA.

Moradi and Shirani[40] calculated the mean number of SSB and DSB induced by both direct and indirect mechanisms for some widely utilized AE emitters (^{67}Ga, ^{99m}Tc, ^{111}In, ^{123}I, ^{125}I, and ^{201}Tl) and a beta-particle emitter (^{131}I), as well as an alpha-particle emitter (^{211}At). The findings demonstrate that the structural form of the sugar-phosphate backbone may significantly influence the frequency of SSBs and DSBs in DNA. Moreover, they stated that the ^{201}Tl and ^{125}I radioisotopes, unlike therapeutic ones, demonstrated the most influence on the quantity of SSBs and DSBs, respectively.

Adjei et al.[41] simulated the radiolytic yields induced by six AEE radionuclides including ^{97}Ru, ^{103}Pd, ^{103m}Rh, ^{111}In, ^{125}I, and ^{131}I in the water model. The study illustrated that the kinetic energies emitted by the electrons affect the transient yield of the radiolytic species. They indicate that nearly all AEE radioisotopes, with the exception of ^{131}I, deliver a higher energy deposition in their vicinity resulting in the induction of a high density of spurs to interact with the medium.

Maria et al.[42] studied the dosimetric behavior of ^{99m}Tc and ^{125}I at nanoscale, given the DNA-intercalation properties of Acridine Orange. They showed that the two classes of compounds can induce DNA DSB, but the DSB yield strongly depends on the linker used to attach the AE emitters to the Acridine Orange moiety.

In a study by Moradi and Shirani on the cell scale[3], the *S*-values for six AE emitters (^{67}Ga, ^{99m}Tc, ^{111}In, ^{123}I, ^{125}I, and ^{201}Tl) and two targeted radionuclide therapy, including ^{131}I and ^{211}At, incorporated into three varied geometric cell configurations were evaluated using Geant4-DNA. Moreover, they presented the mean frequency of SSBs and DSBs attributable to both direct and indirect effects associated with the radionuclides. The findings indicated that at the cellular level, the S-values for the AEE radionuclides were predominantly higher than those for the therapeutic radionuclides ^{131}I but lower than those for ^{211}At. At the DNA level, simulations were

conducted using two distinct geometries of the DNA molecule, and the results were compared with each other. The findings further highlighted that the geometry configuration of the sugar-phosphate groups significantly influences the rate of DNA strand breaks.

Shamsaei Zafarghandi et al.[11] provided a detailed calculation of DNA damage by six AE emitters at the cellular scale, using the Geant4-DNA toolkit. They showed that the significant damage is identified at a distance of about 2.5 nm between an AE emitter atom and the target DNA, with a consequent 50% reduction in damage observed when the distance extends to approximately 3.5 to 4 nm.

Furthermore, some attempts have been devoted to the investigation of DNA damage induced by therapeutic proton beams using an atomic DNA model (such as Chen et al. and Ebrahimi Loshab et al. studies). Accordingly, in this study, we considered several widely-used AEE radionuclides in TRT, including ^{99m}Tc, ^{111}In, ^{123}I, ^{125}I, and ^{201}Tl[11,42–47].

The present study was conducted in two steps. The initial stage entailed the validation of the Geant4-DNA MCS code for cellular dosimetry and DNA damage prediction was performed by comparing its estimation of *S*-values, as well as SSBs and DSBs in the spherical cell geometry with the MIRD database and literature. Then, in the second step, by simulating two adjacent cells containing DNA fragments in their nucleus, the calculations of DNA damage caused by AEE radionuclides (^{99m}Tc, ^{111}In, ^{123}I, ^{125}I, and ^{201}Tl) were carried out at different distances between the two cells. One of the cells was considered to be the source of ionizing radiation and the other was taken as the target. Considering the cell nucleus (N) as the target, these radionuclides were considered to be uniformly distributed across the entire cell (C), on the cell surface (CS), within the cytoplasm (Cy), or specifically in the nucleus (N).

Materials and methods

The MC code Geant4-DNA version 11.1.1 has been used to simulate the interactions of particles at the molecular scale. In the present study, two homogeneous spheres of unit-density liquid water were considered for cell modeling. Based on the typical dimensions for lymphocytes and the V79 Chinese hamster cells[48] and also the MIRD report[49], the radius of the cell and its nucleus was chosen to be 5 and 4 μm, respectively. The electron spectra of the five AEE radionuclides (Table 1) were taken from AAPM report No. 2[43]. For the assessment of electronic emissions' effects on DNA damage, we only focused on AE emissions with a probability greater than 0.001, whereas photon emissions were neglected. Photon emissions generally do not produce a high density of ionizations in the cellular environment at energies relevant to auger therapy; thus, their emissions are considered negligible for cellular dosimetric purposes[49–51]. Energy sampling of AEs from each radioisotope was performed using the G4GeneralParticleSource (GPS) class. For each radioisotope, we implemented a user-defined histogram energy distribution to represent the distinct AEE radioisotope spectrum. This methodology ensures that the sampled electron energies accurately the distinct energy spectrum of AEE from each radioisotope, preserving both the precise energy values and their corresponding emission probabilities. Each characteristic AE energy line was represented in the histogram, with the yield of each bin corresponding to the relative emission probability of that specific auger transition. Taking either the cell nucleus or the entire cell as the target, the AEE radionuclides were assumed to be uniformly distributed - as random emission points - within C, CS, Cy, and N. Then for verification purposes, the self-dose results - based on the *S*-values criteria – were calculated for five source-target (target←source) combinations including *S*(C←C), *S*(C←CS), *S*(N←N), *S*(N←Cy), and *S*(N←CS), which is similar to our previous work[47]. In this way, the mean absorbed dose to a target region r_T from cumulated activity in a source region r_S is given by

$$\bar{D}\,(r_T \leftarrow r_S) = A_c S(r_T \leftarrow r_S) \tag{1}$$

where A_c is the cumulative activity in the source region r_S, and $S(r_T \leftarrow r_S)$ is the absorbed dose to the target region r_T per unit cumulative activity in the source region r_S. $S(r_T \leftarrow r_S)$, which is known as *S*-value (in unit Gy/Bq·s), is a useful dosimetry-related physical quantity[52].

Our results were compared with the corresponding MIRD data taken from MIRDcell v2.0[44]. After verification of the amount of transferred deposited dose from source to target in the cell, the DNA damage results were verified through a comparison of the results of average SSBs and DSBs reported by literature[11] with our results. In this way, the 1bna model (selected from the Protein Data Bank library), containing 12 base pairs, was simulated in a configuration similar to that of Shamsaei Zafarghandi et al.[11]. The 1bna model was enclosed in a bounding box of liquid water and 10^6 decays were generated with isotropic particle emission.

For the evaluation of the cross-dose situation, where the absorbed dose received from emission by decays in the neighboring cell and its effects on the DNA damage, a second similar cell was located in the positive *x*-axis direction assuming the center of first one at the origin of the Cartesian coordinate. The distances between the surfaces of the two cells were considered to be 0 to 5 μm with a step size of 1 μm (as shown in Fig. 1). The verification of the cross-dose was performed based on our previous work[47]. After verification analysis, the nucleus of the cells was filled with 125,000 chromatin fibers which were randomly distributed in the spherical regions. Construction of chromatin fiber was done based on the studies of Bernal and co-workers[39] and Ahmadi Ganjeh and co-workers[53]. In this way, the nucleotide pair was defined as a base pair (bp), which consists of 63 atoms. The properties of the atoms such as chemical element, position, and base of nitrogen were chosen according to the information provided by Bernal and co-workers[39]. Following a double helix of 154 bps (Fig. 2-a) constructed by rotating each bp by +36°, the nucleosome was made by folding two double-helical loops around a histone sphere (Fig. 2-b). The histone protein has a positive charge that reacts with the phosphate groups of the DNA with a negative charge. Histones prevent DNA binding and protect against DNA damage. After the nucleosome, chromatin fiber was made by a helix with 6 nucleosomes (Fig. 2-c), and by repeating this chromatin

Process	Energy	Yield	Process	Energy	Yield
^{99m}Tc			^{125}I		
CK NNX	0.0334	1.98	CK OOX	0.006	3.66
CK LLX	0.0429	0.0193	CK NNX	0.0299	3.51
CK MMX	0.116	0.747	Auger NXY	0.0324	10.9
Auger MXY	0.226	1.1	CK MMX	0.127	1.44
IC 1 M, N…	1.82	0.991	CK LXX	0.219	0.264
Auger LMM	2.05	0.0868	Auger MXY	0.461	3.28
Auger LMX	2.32	0.0137	Auger LMM	3.05	1.25
Auger LXY	2.66	0.0012	IC 1 K	3.65	0.797
Auger KLL	15.3	0.0126	Auger LMX	3.67	0.34
Auger KLX	17.8	0.0047	Auger LXY	4.34	0.0211
IC 2 K	119	0.0843	Auger KLL	22.4	0.138
IC 3 K	122	0.0059	Auger KLX	26.4	0.059
IC 2 L	137	0.0136	Auger KXY	30.2	0.0065
IC 2 M, N…	140	0.0037	IC 1 L	30.6	0.11
IC 3 L	140	0.0025	IC 1 M, N…	34.7	0.0284
^{111}In			^{201}Tl		
Auger NXY	0.00847	7.82	Auger OXY	0.0161	17.6
CK NNX	0.0388	2.54	CK OOX	0.0453	2.84
CK MMX	0.125	0.915	Auger NXY	0.0644	7.93
CK LLX	0.183	0.151	CK NNX	0.172	4.41
Auger MXY	0.35	2.09	CK MMX	0.406	0.923
Auger LMM	2.59	0.835	CK LLX	0.773	0.322
Auger LMX	3.06	0.19	IC 1 M, N…	0.895	0.608
Auger LXY	3.53	0.0109	Auger MXY	1.83	2.03
Auger KLL	19.1	0.103	Auger LMM	7.58	0.541
Auger KLX	22.3	0.0394	Auger LMX	9.85	0.235
Auger KXY	25.5	0.0036	Auger LXY	12	0.0191
IC 1 K	145	0.0824	IC 2 L	12.2	0.0022
IC 1 L	167	0.01	IC 3 L	15.9	0.0861
IC 1 M, N…	171	0.0014	IC 4 L	17.4	0.0724
IC 2 K	219	0.0521	IC 3 M, N…	27.7	0.0236
IC 2 L	241	0.0091	IC 4 M, N…	29.4	0.0237
IC 2 M, N…	245	0.0019	IC 5 K	52.2	0.0797
^{123}I			Auger KLL	55	0.0268
CK NNX	0.0298	2.1	Auger KLX	66.3	0.0153
Auger NXY	0.0325	6.54	Auger KXY	77.5	0.0015
CK MMX	0.127	0.869	IC 6 K	82.8	0.0025
CK LLX	0.213	0.156	IC 7 K	84.3	0.159
Auger MXY	0.461	1.97	IC 5 L	121	0.0152
Auger LMM	3.04	0.751	IC 5 M, N…	133	0.0027
Auger LMX	3.66	0.202	IC 7 L	153	0.0269
Auger LXY	4.28	0.013	IC 7 M, N…	165	0.0094
Auger KLL	22.4	0.0838			
Auger KLX	26.3	0.0384			
Auger KXY	30.2	0.0035			
IC 2 K	127	0.13			
IC 1 L	154	0.0179			
IC 1 M, N…	157	0.0053			

Table 1. Average electron energies (in keV) and yields (per decay) of AEE radionuclides used in the simulations (taken from[43]).

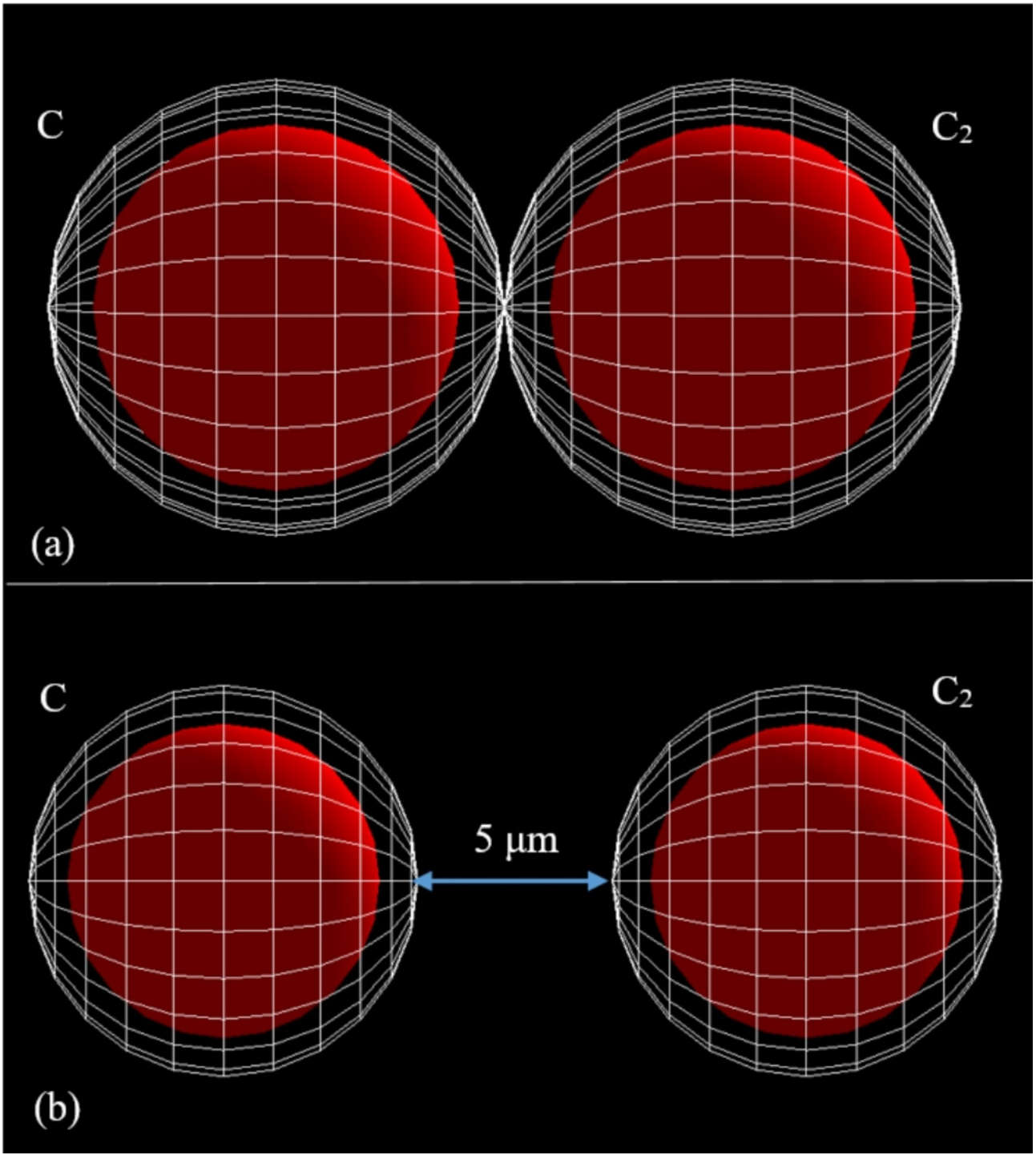

Fig. 1. The model depicts the spherical geometry of a simulated cell using the Geant4-DNA toolkit. The cell has a radius of 5 µm shown in white, with a nucleus of 4 µm radius depicted in red. In (**a**), the surface of cell C is on the surface of cell C_2 (the distance between cells is zero), and in (**b**) the distance between the surfaces of the two cells is 5 µm.

fiber structure, the cell nucleus was simulated (Fig. 2-d). A visualization of the simulated model is provided in Fig. 1-a. In the cross-dose case, four configurations were considered for the evaluation of DNA damages: (N_2←C), (N_2←CS), (N_2←N), and (N_2←Cy). In all the stages of the simulation, the cell C (the first/original cell) was selected as the source. A visualization of the simulated model is provided in Fig. 1-b.

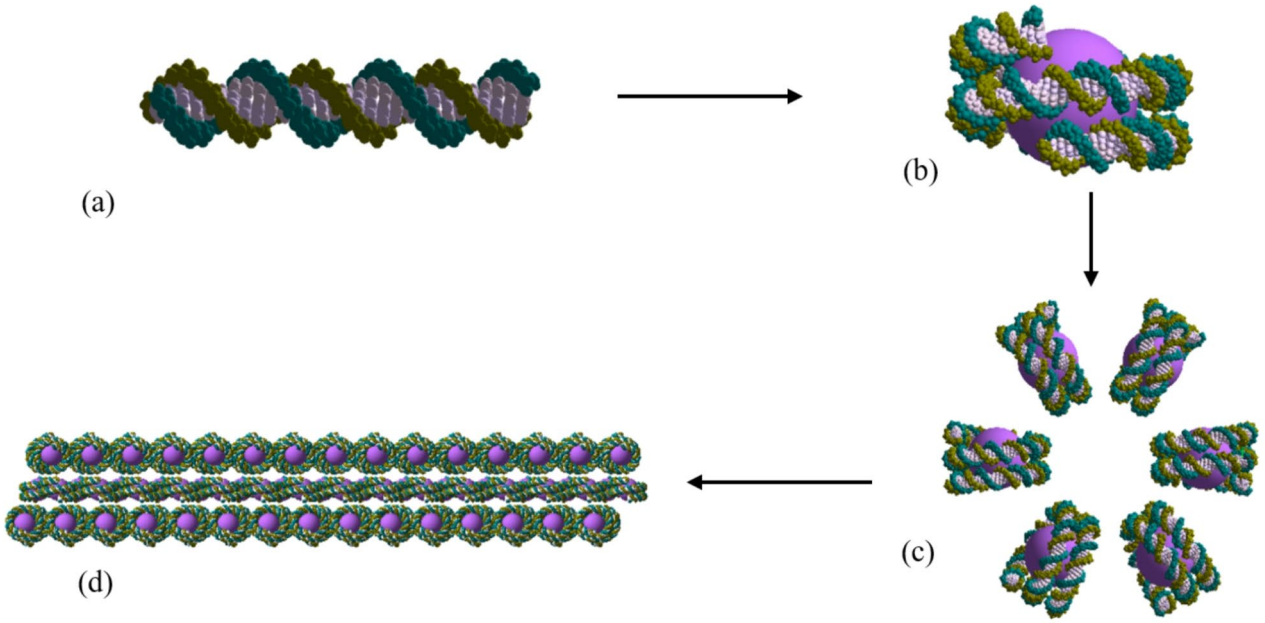

Fig. 2. 3D view of different parts (**a**–**d**) that constructed in the Geant4 toolkit in the present study. (**a**). B-DNA double-helix. (**b**) The nucleosome, two helical loops are folded around a histone. (**c**) Fragment of a chromatin fiber - containing six nucleosomes. (**d**) A chromatin fiber consists of 15 sets of fragments.

Calculation of DNA strand breaks

From a computational perspective, DNA damage from an AEE radiation source can occur through both direct and indirect mechanisms. Direct damage originates from disrupting the DNA structure because of energy deposition in direct hits. It is generally accepted that if the energy deposited in the DNA structure exceeds the threshold value of 8.22 eV, SSBs will occur. DSB is counted when two SSBs happen on the two strands with a distance of less than 10 base pairs. Moreover, HDSB is counted when two SSBs happen (one SSB directly and one SSB indirectly) on the two strands with a distance of less than 10 base pairs. For consideration of DNA damage simulation by direct interaction, we utilized the G4EmDNAPhysics_option6 model. This model enables us to simulate some physical processes such as ionization (relativistic binary encounter Bethe model from CPA100 code (11 eV- 256 keV)), electronic excitation (inelastic) (Dielectric model from CPA100 code (11 eV- 256 keV)), elastic scattering (independent atom method model from CPA100 code ((11 eV- 256 keV)), vibrational excitation (inelastic sub-excitation) and attachment (inelastic sub-excitation) for electrons. The default tracking cut for this model is 11 eV. In the recent study by Zein et al.[54], an update of the Geant4-DNA physics constructor "option 6", including electron interactions with all constituents of the DNA molecule in addition to those already publicly available for liquid water, is introduced. Zein and co-workers expanded electron interactions in Geant4-DNA beyond just water to also include DNA constituents. Besides, they introduced a new sampling method to estimate secondary electron energy without the need for the classical interpolation method that requires large differential cross-section data tables. Considering the physical interactions of particles down to energies of about eV, recording and presenting details of interactions, accumulation energy and coordinates of primary and secondary particles are among the other capabilities of the Geant4-DNA code. Hence, this physics list has been used for the interactions of the electrons with the DNA.

Furthermore, in indirect DNA damage (chemical stage), radiation interacts with water molecules in the medium. Indeed, the interactions produce reactive species, known as free radicals, like hydroxyl radicals (OH), hydrogen peroxide (H_2O_2), hydrogen atoms (H^+), and superoxide radical anions (O_2^-) to damage the DNA indirectly. Among these, OH radicals have the highest capacity to interact with sugar and base groups of the DNA[55]. In this study, we used the G4EmDNAChemistry_option3 physics lists with independent reaction times (IRT) to estimate the indirect DNA damage by considering only OH radicals with a probability of 13% (P_{OH} = 13%) in the target volume[11]. The energy threshold of 8.22 eV is generally considered for evaluating both direct and indirect DNA damage mechanisms. By considering both the direct physical and indirect chemical stages, computational models can provide insights into the fundamental mechanisms of radiation-induced DNA damage and how damage levels correlate with initial radiation exposure conditions. The number of primary particles simulated was 10^6 electrons and the statistical error in the results was less than 2%.

Results

In the present work, the number of SSBs, DSBs, and HDSBs were calculated using Geant4-DNA in one- and two-cell configurations. At first, the self-dose and cross-dose results were verified through comparison with the corresponding MIRD data taken from MIRDcell v2.0[44] for ^{99m}Tc, ^{111}In, ^{123}I, ^{125}I, and ^{201}Tl radionuclides. The average difference between this work and MIRDcell was about 2%, showing good agreement. At the second step of the verification, the direct and indirect SSBs and DSBs of the 1bna model (as shown in Fig. 3) irradiated with four radionuclides (^{99m}Tc, ^{111}In, ^{123}I, and ^{125}I) originating from the physical and chemical stages were compared with the values reported by Shamsaei Zafarghandi[11]. The total number of SSBs (direct and indirect) per decay reported by Shamsaei Zafarghandi (this work) at a distance of 2.5 nm were 3.20 (3.36), 2.80 (2.90), 1 (1.05), and 1 (1.06) for ^{125}I, ^{111}In, ^{99m}Tc, and ^{123}I, respectively. The results for DSBs were 1.70 (1.91), 1.39 (1.20), 0.50 (0.51), and 0.50 (0.52), respectively. Generally, there is a good agreement between the results since the average magnitude of the differences is below 5% and 8% for SSBs and DSBs, respectively.

For one-cell configuration, all types of DNA break inside the cell nucleus (N) were calculated from radioactivity in C, CS, Cy, and N, i.e. in the case of (N←C), (N←CS), (N←Cy), and (N←CS) combinations. In all cases, the target was N containing 125,000 chromatin fibers (1.7325 Gbps). Figure 4 shows the number of direct and indirect SSBs per event for each radionuclide across the different source-target combinations. It can be seen that the obtained SSBs are different depending on the AEE radionuclides. This is because radionuclides are unique in their energy spectrum and differ from each other in the number of electron emission processes, the decay spectra, and the total yield of Auger + CK + IC electrons per decay[43]. The results in all combinations show that ^{201}Tl and ^{125}I have the greatest impact on the number of SSBs. Comparison of ^{201}Tl and other radioisotopes showed that the SSB values of the ^{201}Tl were 6.23%, 36%, 38.7%, and 45% higher than ^{125}I, ^{123}I, ^{111}In, and ^{99m}Tc, respectively, in the case of (N←N) source-target combination. These values are 5.66%, 35.9%, 37.7%, and 44.5% for (N←Cy), 5.38%, 34%, 38.1%, and 43.8% for (N←C), and 2.0%, 7.7%, 14.8% and 17.36% for (N←CS), in comparison to the SSB values of ^{125}I, ^{123}I, ^{111}In, and ^{99m}Tc, respectively. On the other hand, the SSB in the case of (N←N) for ^{201}Tl is 23.8%, 22.6%, and 78.2% higher than the situation where AEE radioisotopes are distributed in the (N←C), (N←Cy), and (N←CS).

Figure 5 presents the number of direct and indirect DSBs per event for each radionuclide, considering different target←source combinations. ^{201}Tl was found to be significantly more effective than ^{125}I, ^{123}I, ^{111}In, and ^{99m}Tc with 18.3%, 38.2%, 44%, and 55% higher DSB values, respectively, in the (N←N) combination. For the (N←Cy) combination, these values were 9.5%, 37.6%, 42.6%, and 44.9%. Furthermore, in the (N←C) combination, the values stood at 9%, 38.2%, 41.1%, and 48.8%, while in the (N←CS) combination, they were

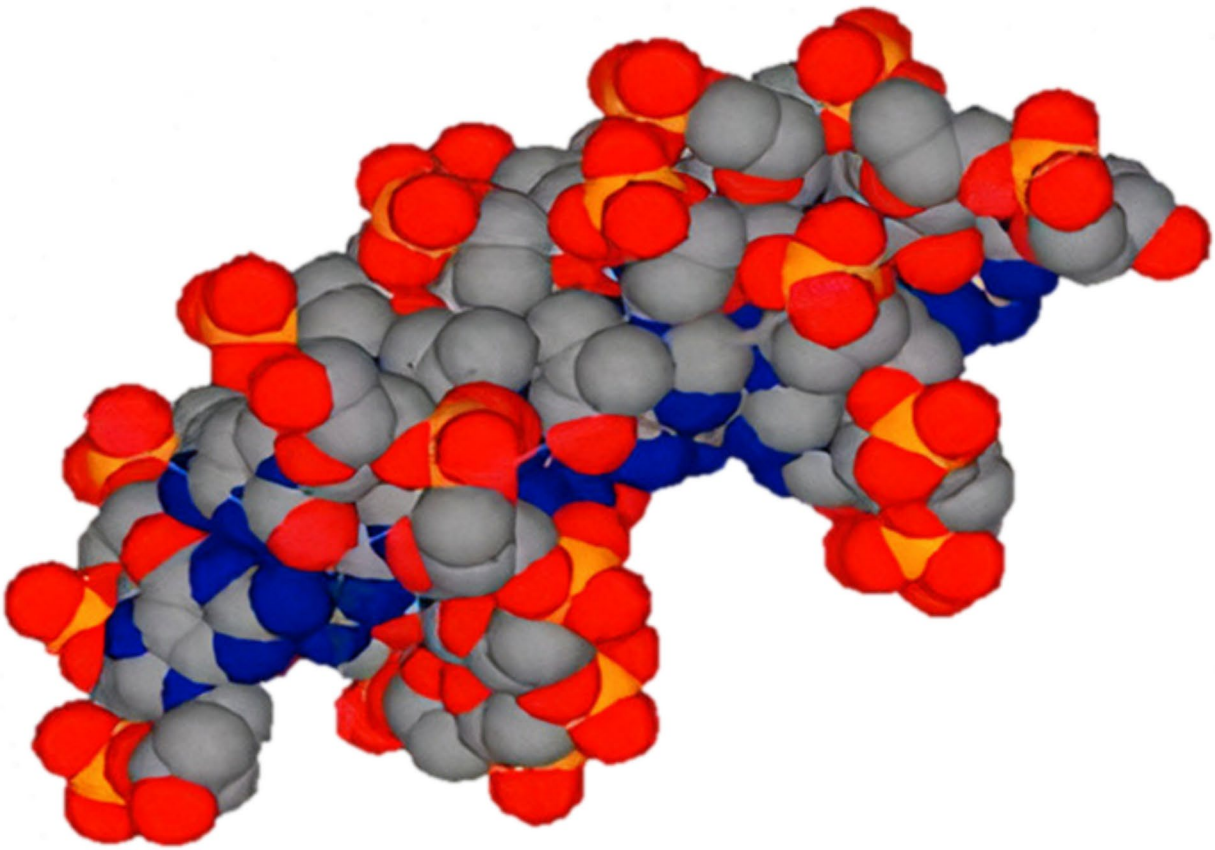

Fig. 3. OpenGL visualization of the 1bna model.

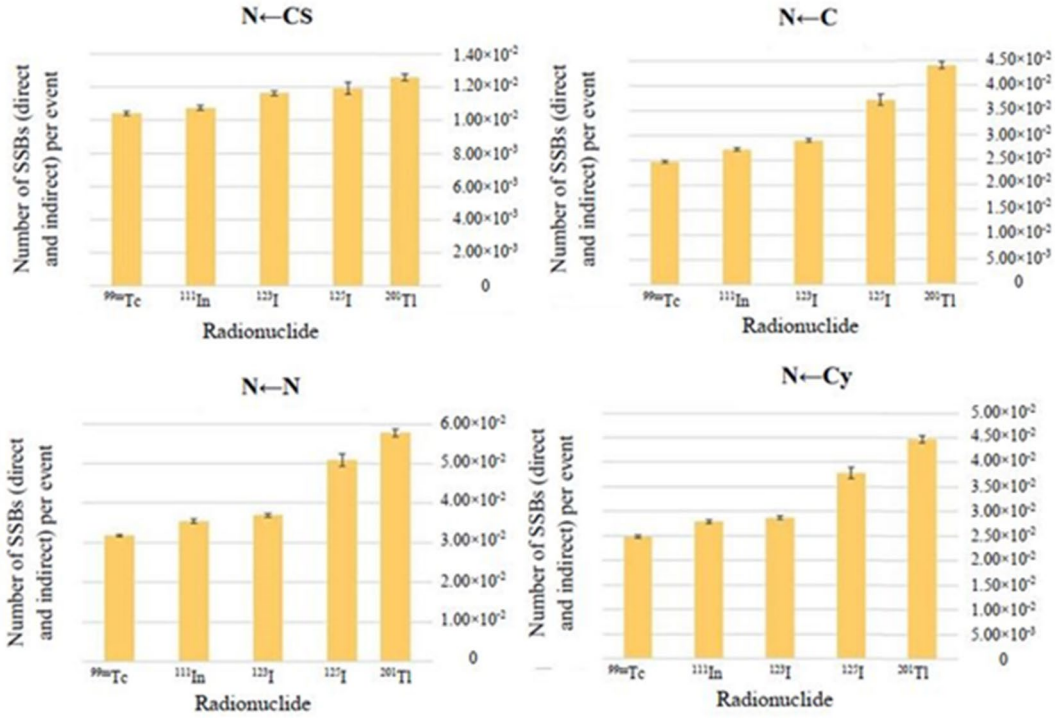

Fig. 4. Number of SSBs (Direct and Indirect) per event for ^{201}Tl, ^{125}I, ^{123}I, ^{111}In, and ^{99m}Tc for the following target←source combinations: (N←CS), (N←C), (N←N), and (N← Cy).

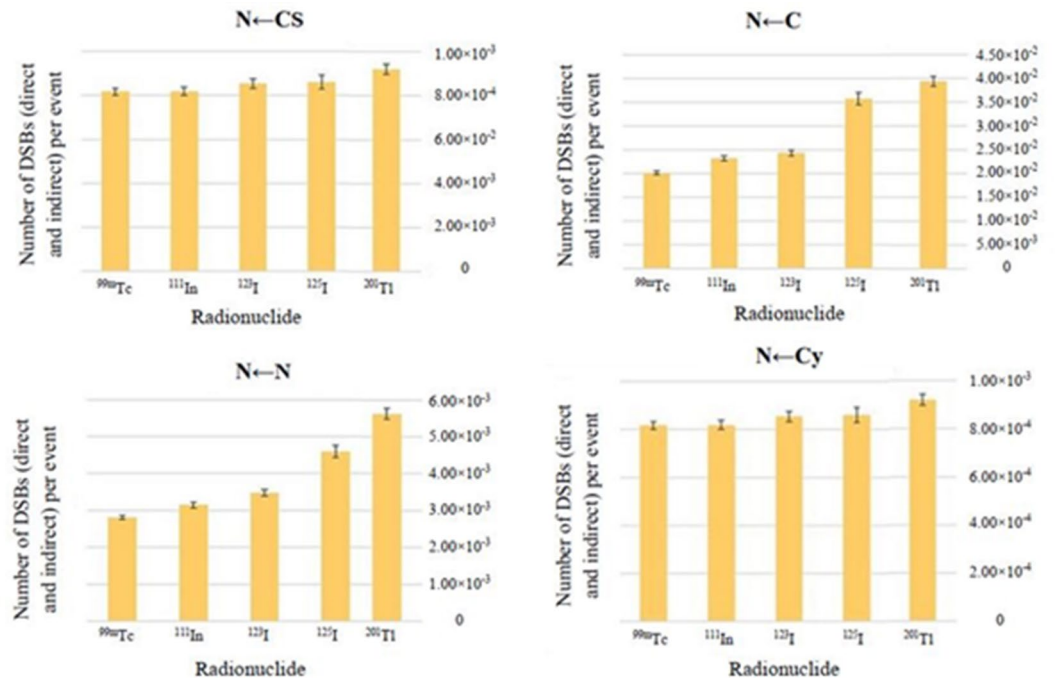

Fig. 5. Number of DSBs (Direct and Indirect) per event for ^{201}Tl, ^{125}I, ^{123}I, ^{111}In, and ^{99m}Tc for the following target←source combinations: (N←CS), (N←C), (N←N), and (N← Cy).

6.5%, 7.2%, 11%, and 11.3%. These values are presented in comparison to the respective DSBs of ^{125}I, ^{123}I, ^{111}In, and ^{99m}Tc. Moreover, the DSB for ^{201}Tl in the case of (N←N) is 26.6%, 25.5%, and 82% higher than the situation where AEE radioisotopes are distributed in the (N←C), (N←Cy), and (N←CS). It is worth noting that from Figs. 4 and 5, the values of the SSBs and DSBs are less different for DNA breaks caused by the AEE radionuclides in the case of (N←Cy) and (N←CS) combinations.

In addition, Figs. 6 and 7 display the HDSB/event and Dose/event for each radionuclide, considering four combinations under study. Compared to ^{201}Tl, the HDSB (Dose) for ^{125}I, ^{123}I, ^{111}In, and ^{99m}Tc respectively, decreased by 32% (8%), 39% (9%), 48% (19%), and 57% (21%) for the (N←CS), by 4% (15%), 27% (36%), 50% (39%), and 38% (45%) for the (N←Cy), by 26% (14%), 49% (36%), 48% (38%), and 57% (45%) for the (N←C), and by 13% (12%), 30% (36%), 52% (39%), and 50% (46%) for the (N←N) combination.

In the next step of the research, the effect of radiation from AE emitters within a cell on the DNA breaks in the neighboring cell for different cell-to-cell distances were examined in an atomic model for ^{99m}Tc, ^{123}I, ^{111}In,^{201}Tl, and ^{125}I (Tables 2, 3, 4 and 5). As a previous procedure, four configurations were considered: (N_2←C), (N_2←CS), (N_2←N), and (N_2←Cy), in which N_2 as the target is the neighboring cell nucleus containing 125,000 chromatin fibers (1.7325 Gbps).

As listed in Tables 6, 7, 8 and 9, we compared DNA damages and dose deposition in target caused by electron emission of ^{99m}Tc, ^{123}I, ^{111}In, ^{201}Tl, and ^{125}I at distances from 0 to 5 μm, approximating the size of a whole cell. In comparison to the 0 μm distance between the two cell surfaces, the DNA breaks and dose deposition in target for ^{99m}Tc, ^{123}I, ^{111}In, ^{201}Tl, and ^{125}I, decreased at 1 to 5 μm distance, respectively.

Discussion

In the first part of the simulations for self-dose inspection, the results obviously demonstrate that in all combinations, the impact of ^{201}Tl > ^{125}I > ^{123}I > ^{111}In > ^{99m}Tc on the DNA damage is significant when the target is N (nucleus of the first spherical cell). These results revealed the highest (lowest) DNA damage score in the cells treated with ^{201}Tl (^{99m}Tc), because of the electron emission spectrum of the ^{201}Tl, ^{125}I, ^{123}I, ^{111}In, and ^{99m}Tc have total decay yields of 37.3971, 25.6591, 14.9067, 14.8548, 5.0663, respectively.

It should be noted that the majority of these decay yields are related to electrons below 1 keV, with values of 34.633, 25.43, 11.633, 5.556, and 3.846, respectively. The significant damage observed at energies below 1 keV in the proximity of DNA is predominantly attributed to AEs and CK transitions originating from the M and N shells, as well as certain transitions within the L shell. On the other hand, the change of the target←source combination from N←N to N←Cy, N←C, or N←CS has led to a considerable reduction in the number of strand breaks. This can be attributed to the high LET of AEE radionuclides and their short range.

We can compare the first six processes detailed in Table 1, including CK OOX, CK NNX, Auger NXY, CK MMX, CK LXX, and Auger MXY, for ^{125}I and ^{201}Tl. In comparison, the energy values of ^{201}Tl are approximately 87%, 83%, 50%, 69%, 71%, and 75% higher than those of ^{125}I in the specified processes. This difference indicates that ^{201}Tl may induce more strand breaks in the sugar-phosphate group of the DNA molecule at shorter distances in N←N to N←Cy, N←C, and N←CS combinations.

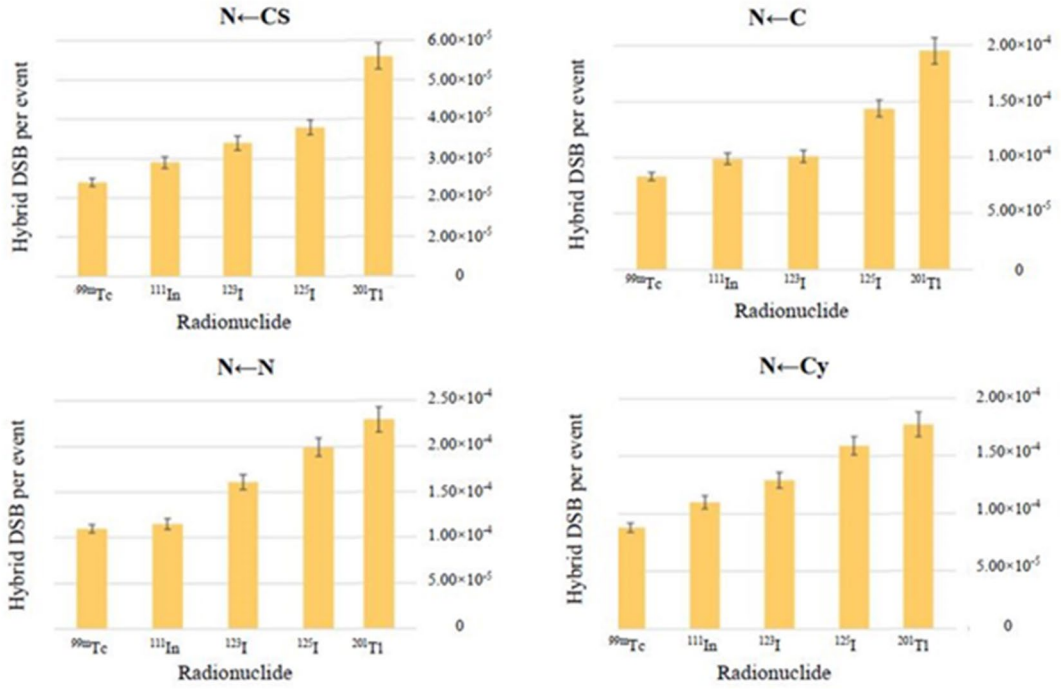

Fig. 6. Number of HDSBs per event for ^{201}Tl, ^{125}I, ^{123}I, ^{111}In, and ^{99m}Tc for the following target←source combinations: (N←CS), (N←C), (N←N), and (N← Cy).

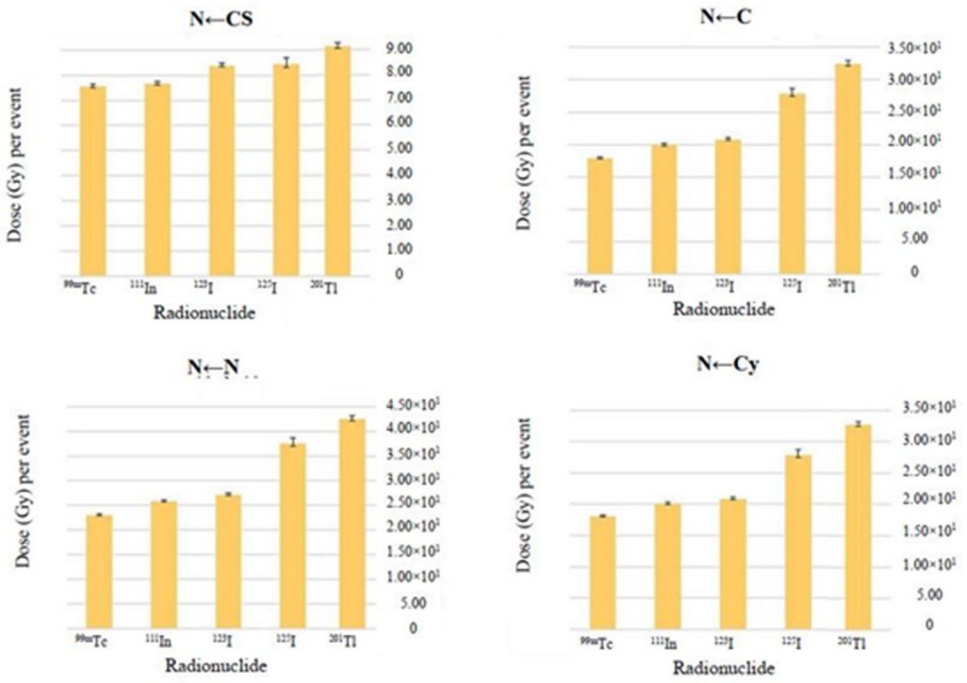

Fig. 7. Dose per event for ^{201}Tl, ^{125}I, ^{123}I, ^{111}In, and ^{99m}Tc for the following target←source combinations: (N←CS), (N←C), (N←N), and (N← Cy).

Both ^{125}I and ^{123}I have similar chemical behavior, suggesting that any variations in their biological effects can be attributed to the differing number of AEE per decay by these radionuclides. However, it is noteworthy that the electron frequencies per decay for ^{125}I are almost double those of ^{123}I, and the most energy of the IC electrons is 35.4 keV (for ^{125}I) as opposed to 159 keV (for ^{123}I). Analyzing the initial four emission processes for ^{123}I (Table 1), including CK NNX, Auger NXY, CK MMX, and Auger MXY. In comparison, it is observed that the energy values of ^{125}I do not significantly differ from that of ^{123}I in the first two processes and remain constant in the last two processes. However, when considering the yields of ^{125}I and ^{123}I, we notice that the yield of ^{125}I is consistently higher about 40% in each case. This discrepancy suggests that ^{125}I may be more effective than ^{123}I since its higher number of emitted electrons can lead to a greater amount of energy deposition.

Additionally, when comparing the radionuclides ^{123}I and ^{111}In, the values for CK MMX, CK LLX, and Auger MXY in ^{123}I are about 2% (5%), 14% (3%), and 25% (6%) higher than those in ^{111}In. It is noted that the energy values (yield) of the initial process CK NNX in ^{123}I are approximately 12% (17%) lower than that of ^{111}In. Furthermore, ^{123}I has one more process with energy below 1 keV including Auger NXY. Hence, the electrons from ^{123}I are absorbed in shorter distances than those emitted from ^{111}In within the DNA molecule, which results in a higher number of strand breaks for ^{123}I in comparison to ^{111}In. Besides, when examining the initial four processes for ^{99m}Tc, including CK NNX, CK LXX, CK MMX, and Auger MXY, compared to ^{111}In, it is evident that the energy values (yield) show an increase of approximately 1% (22%), 7% (87%), 76% (18%), and 35% (47%), respectively.

Moreover, in the second part of the simulations, when changing the target from the nucleus of the first spherical cell (N) to the nucleus of the second spherical cell (N_2) and considering distances ranging from 0 to 5 μm between the surfaces of the two cells, there was a significant shift in the outcomes. As previously discussed, given the high LET and short range of the specified radionuclides, increasing the distance between the cells led to a change in the ranking of their impact on DNA damage from ^{201}Tl > ^{125}I > ^{123}I > ^{111}In > ^{99m}Tc to ^{99m}Tc > ^{123}I > ^{111}In > ^{201}Tl > ^{125}I. Hence, ^{99m}Tc and ^{125}I resulted in the highest and lowest DNA damage. Indeed, the electron decay yields for ^{99m}Tc show that 72% are attributed to electrons below 1 keV, with only 28% associated with electrons above 1 keV. In comparison, for ^{123}I, these proportions are 88% and 12%; for ^{111}In, 91% and 9%; for ^{201}Tl, 91% and 9%; and for ^{125}I, 90% and 10%, respectively for electrons below and above 1 keV.

When comparing the potential for DNA damage between ^{99m}Tc and ^{123}I within distances ranging from 0 to 5 μm between the surfaces of the two cells, the data indicates that ^{99m}Tc is more effective due to the higher energy and yield of its AE emissions. ^{99m}Tc emits AEs with higher energies, such as Auger KLL, Auger KLX, and Auger KXY, with relatively high yields. On the other hand, ^{123}I also emits AEs with comparable energies, like Auger KLL and Auger KXY, but their yields are lower than those of ^{99m}Tc. Furthermore, ^{99m}Tc produces higher-energy IC electrons, such as IC 2 K and IC 3 K, while the highest energy of IC emission for ^{123}I belongs to IC 2 K with a lower yield of 0.13, which can also contribute to DNA damage at short ranges. It is important to highlight that ^{99m}Tc has two additional processes (the last two processes for ^{99m}Tc in Table 1) compared to ^{123}I, and both of these processes have energy values of 140 keV. Taken together, the combination of higher energy and higher

Radionuclide	Distance (μm)	SSBs per event (N_2←CS)	DSBs per event (N_2←CS)	HDSB per event (N_2←CS)	Dose per event (Gy) (N_2←CS)
^{99m}Tc	0	2.84×10^{-3}	2.23×10^{-4}	1.20×10^{-5}	1.95
	1	2.24×10^{-3}	1.84×10^{-4}	1.00×10^{-5}	1.58
	2	1.77×10^{-3}	1.55×10^{-4}	1.00×10^{-5}	1.29
	3	1.50×10^{-3}	1.12×10^{-4}	6.00×10^{-6}	1.06
	4	1.27×10^{-3}	8.50×10^{-5}	6.00×10^{-6}	0.873
	5	1.08×10^{-3}	9.30×10^{-5}	5.00×10^{-6}	0.785
^{123}I	0	2.49×10^{-3}	1.82×10^{-4}	1.00×10^{-5}	1.81
	1	1.87×10^{-3}	1.16×10^{-4}	8.00×10^{-6}	1.35
	2	1.41×10^{-3}	1.10×10^{-4}	5.00×10^{-6}	1.06
	3	1.17×10^{-3}	8.60×10^{-5}	4.00×10^{-6}	0.862
	4	9.68×10^{-4}	7.50×10^{-5}	4.00×10^{-6}	0.689
	5	7.80×10^{-4}	8.70×10^{-5}	3.00×10^{-6}	0.604
^{111}In	0	2.18×10^{-3}	1.50×10^{-4}	7.00×10^{-6}	1.57
	1	1.53×10^{-3}	1.08×10^{-4}	6.00×10^{-6}	1.17
	2	1.30×10^{-3}	8.90×10^{-5}	3.00×10^{-6}	0.898
	3	1.02×10^{-3}	7.70×10^{-5}	3.00×10^{-6}	0.732
	4	7.64×10^{-4}	5.40×10^{-5}	3.00×10^{-6}	0.583
	5	7.71×10^{-4}	7.90×10^{-5}	1.00×10^{-6}	0.499
^{201}Tl	0	1.67×10^{-3}	1.36×10^{-4}	6.00×10^{-6}	1.22
	1	1.33×10^{-3}	1.01×10^{-4}	4.00×10^{-6}	0.912
	2	1.03×10^{-3}	7.20×10^{-5}	2.00×10^{-6}	0.734
	3	7.94×10^{-4}	6.00×10^{-5}	1.00×10^{-6}	0.582
	4	6.29×10^{-4}	3.20×10^{-5}	1.00×10^{-6}	0.443
	5	5.62×10^{-4}	3.90×10^{-5}	0	0.392
^{125}I	0	1.58×10^{-3}	1.35×10^{-4}	3.00×10^{-6}	1.22
	1	1.14×10^{-3}	8.20×10^{-5}	1.00×10^{-6}	0.876
	2	7.06×10^{-4}	6.50×10^{-5}	1.00×10^{-6}	0.538
	3	5.05×10^{-4}	4.30×10^{-5}	1.00×10^{-6}	0.385
	4	3.56×10^{-4}	2.20×10^{-5}	0	0.244
	5	2.46×10^{-4}	7.00×10^{-5}	0	0.169

Table 2. The number of strand breaks and dose per event for ^{99m}Tc, ^{123}I, ^{111}In, ^{201}Tl, and ^{125}I in the case of (N_2←CS) combination.

yield Auger and IC emissions from ^{99m}Tc causes more DNA damage than ^{123}I within distances ranging from 0 to 5 μm between the surfaces of the two cells.

When comparing ^{99m}Tc to ^{111}In, it is evident that ^{99m}Tc emits several high-energy AEs with significantly higher yields. For instance, ^{99m}Tc emits Auger KLL, Auger KLX, and Auger KXY, while ^{111}In emits Auger KLL and Auger KLX with lower yields. Additionally, ^{99m}Tc emits higher energy IC electrons, such as IC 2 K and IC 3 K, compared to the highest yield of IC emission for ^{111}In which belongs to IC 1 K.

In comparison to ^{201}Tl, while it emits high-energy AEs like Auger KLL and Auger KLX, ^{99m}Tc emits similar high-energy AEs with significantly higher yields. Additionally, ^{99m}Tc emits high-energy IC electrons like IC 2 K and IC 3 K with higher yields compared to ^{201}Tl which emits IC 5 K. The cumulative effect of numerous high-energy Auger and IC emissions with significantly higher yields in of ^{99m}Tc suggests a greater potential to cause DNA damage compared to ^{201}Tl.

Regarding the comparison between ^{99m}Tc and ^{125}I in terms of potential DNA damage within distances ranging from 0 to 5 μm between the surfaces of the two cells, data indicates that ^{99m}Tc is more effective due to its emission of higher energy AEs and IC electrons with higher yields. ^{99m}Tc emits several high-energy AEs with significantly higher yields compared to ^{125}I, such as Auger KLL, Auger KLX, and Auger KXY. On the other hand, ^{125}I emits Es like Auger KLL and Auger KLX with lower yields. Additionally, ^{99m}Tc emits higher energy IC electrons with higher yields, such as IC 2 K and IC 3 K, compared to the highest energy of IC emission for ^{125}I which belongs to IC 2 K.

Furthermore, the results indicate that ^{123}I emits more high-energy AEs compared to ^{111}In. For example, ^{123}I emits Auger KLL, Auger KLX, and Auger KXY with higher yields, respectively. In contrast, the Auger emissions with the highest energy in the case of ^{111}In, such as Auger KLL and Auger KLX, have lower yields. Additionally, ^{123}I emits a higher energy IC electron, IC 2 K, while the highest energy of IC emission for ^{111}In belongs to IC 1 K.

The data further reveals that ^{111}In emits higher energy AEs compared to ^{201}Tl, such as Auger KLL, Auger KLX, and Auger KXY (25.5 keV). Although ^{201}Tl emits AEs like Auger KLL (55.0 keV) and Auger KLX (66.3 keV), their higher energies suggest longer ranges and potentially less energy deposition within distances ranging from

Radionuclide	Distance (μm)	SSBs per event (N_2←Cy)	DSBs per event (N_2←Cy)	HDSB per event (N_2←Cy)	Dose per event (Gy) (N_2←Cy)
^{99m}Tc	0	2.74×10^{-3}	2.15×10^{-4}	1.40×10^{-5}	1.92
	1	2.21×10^{-3}	1.68×10^{-4}	1.30×10^{-5}	1.55
	2	1.74×10^{-3}	1.18×10^{-4}	1.10×10^{-5}	1.27
	3	1.46×10^{-3}	1.16×10^{-4}	9.00×10^{-6}	1.06
	4	1.27×10^{-3}	1.12×10^{-4}	6.00×10^{-6}	0.908
	5	1.03×10^{-3}	1.00×10^{-4}	4.00×10^{-6}	0.773
^{123}I	0	2.41×10^{-3}	1.99×10^{-4}	1.40×10^{-5}	1.70
	1	1.94×10^{-3}	1.12×10^{-4}	1.30×10^{-5}	1.33
	2	1.55×10^{-3}	1.07×10^{-4}	1.10×10^{-5}	1.05
	3	1.17×10^{-3}	1.05×10^{-4}	9.00×10^{-6}	0.833
	4	9.79×10^{-4}	7.60×10^{-5}	6.00×10^{-6}	0.691
	5	8.91×10^{-4}	7.00×10^{-5}	4.00×10^{-6}	0.609
^{111}In	0	2.12×10^{-3}	1.55×10^{-4}	6.00×10^{-6}	1.50
	1	1.64×10^{-3}	1.00×10^{-4}	5.00×10^{-6}	1.13
	2	1.29×10^{-3}	9.40×10^{-5}	4.00×10^{-6}	0.876
	3	9.67×10^{-4}	9.10×10^{-5}	4.00×10^{-6}	0.714
	4	7.48×10^{-4}	6.60×10^{-5}	3.00×10^{-6}	0.560
	5	6.46×10^{-4}	6.00×10^{-5}	2.00×10^{-6}	0.496
^{201}Tl	0	1.68×10^{-3}	1.32×10^{-4}	4.00×10^{-6}	1.20
	1	1.17×10^{-3}	8.90×10^{-5}	3.00×10^{-6}	0.862
	2	9.39×10^{-4}	6.80×10^{-5}	3.00×10^{-6}	0.710
	3	7.89×10^{-4}	5.20×10^{-5}	3.00×10^{-6}	0.553
	4	6.02×10^{-4}	4.50×10^{-5}	2.00×10^{-6}	0.460
	5	5.53×10^{-4}	3.80×10^{-5}	1.00×10^{-6}	0.401
^{125}I	0	1.62×10^{-3}	1.17×10^{-4}	3.00×10^{-6}	1.16
	1	1.04×10^{-3}	7.60×10^{-5}	2.00×10^{-6}	0.770
	2	7.55×10^{-4}	5.50×10^{-5}	2.00×10^{-6}	0.485
	3	5.31×10^{-4}	2.40×10^{-5}	1.00×10^{-6}	0.328
	4	3.11×10^{-4}	1.50×10^{-5}	1.00×10^{-6}	0.211
	5	2.53×10^{-4}	1.40×10^{-5}	0	0.162

Table 3. The number of strand breaks and dose per event for ^{99m}Tc, ^{123}I, ^{111}In, ^{201}Tl, and ^{125}I in the case of (N_2←Cy) combination.

0 to 5 μm between the surfaces of the two cells. ^{111}In also emits IC electrons with higher yields like IC 1 K (145 keV, yield 0.0824) compared to the highest yield of IC emission for ^{201}Tl which belongs to IC 5 K (52.2 keV, yield 0.0797).

Moreover, the data indicates that ^{201}Tl emits several AEs with higher energies compared to ^{125}I, such as Auger KLL (55.0 keV), Auger KLX (66.3 keV), and Auger KXY (77.5 keV). While ^{125}I emits AEs like Auger KLL (22.4 keV) and Auger KLX (26.4 keV), which their lower energies imply a shorter range and potentially less energy deposition within 5 micrometers. Additionally, ^{201}Tl emits higher energy IC electrons like IC 5 K (52.2 keV) and IC 5 L (121 keV), whereas the highest energy of IC emission for ^{125}I belongs to IC 2 K (127 keV). The higher energy emissions from ^{201}Tl, particularly the numerous high-energy AEs, suggest a greater potential to cause DNA damage compared to ^{125}I when there is a distance of 0 to 5 μm between the surfaces of the two cells.

Conclusion

In this study, we used the Geant4-DNA MC code to investigate the direct and indirect DNA damage induced by AEE radionuclides for targeted cancer therapy applications. An atomic DNA model was constructed and the numbers of SSBs, DSBs, HDSBs, and dose per event were calculated for five theranostic radionuclides (^{99m}Tc, ^{111}In, ^{123}I, ^{125}I, and ^{201}Tl) at distances of 0–5 μm from the DNA target. In the case where the cell nucleus of C cell (N) was selected as the target in combinations such as (N←C), (N←CS), (N←Cy), and (N←CS), the obtained results demonstrate that ^{201}Tl produces the most DNA damage, with up to 6.23%, 36%, 38.7%, and 45% higher SSBs compared to ^{125}I, ^{123}I, ^{111}In, and ^{99m}Tc, respectively. ^{201}Tl also showed the highest dose deposition, approximately 46% greater than ^{99m}Tc. However, based on the results, in all combinations where the cell nucleus of C_2 cell (N_2) was selected as the target (N_2←C), (N_2←CS), (N_2←Cy), and (N_2←CS),^{99m}Tc and ^{201}Tl cause the highest and the lowest DNA damage, respectively. This change can be attributed to the emission of higher energy Auger and IC electrons with higher yields from ^{99m}Tc. So, although ^{201}Tl caused more damage than ^{99m}Tc at 0 μm in the first part of the simulations, increasing the target distance to 5 μm in part two allowed ^{99m}Tc to overtake

Radionuclide	Distance (μm)	SSBs per event (N_2←C)	DSBs per event (N_2←C)	HDSB per event (N_2←C)	Dose per event (Gy) (N_2←C)
^{9m}Tc	0	2.68×10^{-3}	1.71×10^{-4}	8.00×10^{-6}	1.88
	1	2.04×10^{-3}	1.62×10^{-4}	7.00×10^{-6}	1.53
	2	1.81×10^{-3}	1.23×10^{-4}	7.00×10^{-6}	1.25
	3	1.57×10^{-3}	1.03×10^{-4}	4.00×10^{-6}	1.05
	4	1.23×10^{-3}	9.00×10^{-5}	3.00×10^{-6}	0.913
	5	1.08×10^{-3}	8.30×10^{-5}	1.00×10^{-6}	0.762
^{123}I	0	2.38×10^{-3}	1.60×10^{-4}	6.00×10^{-6}	1.66
	1	1.74×10^{-3}	1.50×10^{-4}	4.00×10^{-6}	1.26
	2	1.52×10^{-3}	9.10×10^{-5}	4.00×10^{-6}	1.03
	3	1.13×10^{-3}	9.00×10^{-5}	3.00×10^{-6}	0.842
	4	1.01×10^{-3}	8.40×10^{-5}	1.00×10^{-6}	0.702
	5	7.40×10^{-4}	4.30×10^{-5}	1.00×10^{-6}	0.588
^{111}IN	0	1.89×10^{-3}	1.43×10^{-4}	5.00×10^{-6}	1.39
	1	1.46×10^{-3}	1.22×10^{-4}	4.00×10^{-6}	1.07
	2	1.17×10^{-3}	8.90×10^{-5}	3.00×10^{-6}	0.828
	3	9.65×10^{-4}	6.80×10^{-5}	2.00×10^{-6}	0.684
	4	8.16×10^{-4}	6.60×10^{-5}	1.00×10^{-6}	0.589
	5	6.91×10^{-4}	4.20×10^{-5}	1.00×10^{-6}	0.498
^{201}Tl	0	1.54×10^{-3}	1.15×10^{-4}	4.00×10^{-6}	1.07
	1	1.11×10^{-3}	8.10×10^{-5}	3.00×10^{-6}	0.832
	2	9.25×10^{-4}	5.50×10^{-5}	1.00×10^{-6}	0.674
	3	7.73×10^{-4}	5.40×10^{-5}	0	0.594
	4	6.05×10^{-4}	5.20×10^{-5}	0	0.459
	5	5.86×10^{-4}	2.80×10^{-5}	0	0.405
^{125}I	0	1.47×10^{-3}	1.02×10^{-4}	2.00×10^{-6}	1.10
	1	1.05×10^{-3}	7.60×10^{-5}	1.00×10^{-6}	0.736
	2	6.64×10^{-4}	4.40×10^{-5}	1.00×10^{-6}	0.476
	3	4.51×10^{-4}	2.70×10^{-5}	0	0.311
	4	3.09×10^{-4}	2.50×10^{-5}	0	0.215
	5	2.02×10^{-4}	2.30×10^{-5}	0	0.154

Table 4. The number of strand breaks and dose per event for ^{99m}Tc, ^{123}I, ^{111}In, ^{201}Tl, and ^{125}I in the case of (N_2←C) combination.

^{201}Tl and cause the most DNA strand breaks. Analysis of SSBs, DSBs, HDSBs, and dose at varying distances revealed a strong distance dependence so that DNA damage and deposited dose decreased rapidly from 0 to 5 μm. Additionally, the (N←N) source-target combination resulted in higher DNA damage compared to other combinations. When examining cell displacement, ^{99m}Tc and ^{123}I caused the most SSBs, while ^{125}I resulted in the least. From 0 to 5 μm cell separation, SSBs decreased by 59.5–89% depending on the radionuclide. Overall, this study demonstrates that Auger radionuclides can induce substantial DNA damage, dependent on radionuclide, distance, and cell geometry factors. The DNA damage quantification and cell distance effects presented provide insights into Auger therapy effectiveness and guide optimization of delivery strategies for targeted cancer treatment.

Radionuclide	Distance (μm)	SSBs per event (N_2←N)	DSBs per event (N_2←N)	HDSB per event (N_2←N)	Dose per event (Gy) (N_2←N)
^{9m}Tc	0	2.54×10^{-3}	1.82×10^{-4}	1.30×10^{-5}	1.83
	1	2.11×10^{-3}	1.68×10^{-4}	9.00×10^{-6}	1.50
	2	1.85×10^{-3}	1.40×10^{-4}	9.00×10^{-6}	1.30
	3	1.34×10^{-3}	1.05×10^{-4}	8.00×10^{-6}	1.05
	4	1.27×10^{-3}	1.04×10^{-4}	8.00×10^{-6}	0.925
	5	1.03×10^{-3}	7.20×10^{-5}	4.00×10^{-6}	0.796
^{123}I	0	2.11×10^{-3}	1.47×10^{-4}	9.00×10^{-6}	1.56
	1	1.72×10^{-3}	1.39×10^{-4}	8.00×10^{-6}	1.23
	2	1.39×10^{-3}	1.23×10^{-4}	6.00×10^{-6}	1.02
	3	1.07×10^{-3}	7.40×10^{-5}	5.00×10^{-6}	0.813
	4	1.00×10^{-3}	6.10×10^{-5}	3.00×10^{-6}	0.683
	5	8.02×10^{-4}	5.90×10^{-5}	2.00×10^{-6}	0.576
^{111}In	0	1.75×10^{-3}	1.41×10^{-4}	8.00×10^{-6}	1.35
	1	1.61×10^{-3}	1.02×10^{-4}	6.00×10^{-6}	1.00
	2	1.12×10^{-3}	7.10×10^{-5}	5.00×10^{-6}	0.812
	3	1.02×10^{-3}	6.10×10^{-5}	5.00×10^{-6}	0.696
	4	8.50×10^{-4}	5.30×10^{-5}	2.00×10^{-6}	0.567
	5	6.99×10^{-4}	4.40×10^{-5}	2.00×10^{-6}	0.482
^{201}Tl	0	1.49×10^{-3}	1.15×10^{-4}	4.00×10^{-6}	1.04
	1	1.05×10^{-3}	8.30×10^{-5}	3.00×10^{-6}	0.823
	2	8.56×10^{-4}	6.80×10^{-5}	2.00×10^{-6}	0.635
	3	7.45×10^{-4}	4.20×10^{-5}	0	0.557
	4	5.99×10^{-4}	4.20×10^{-5}	0	0.458
	5	5.44×10^{-4}	3.90×10^{-5}	0	0.398
^{125}I	0	1.40×10^{-3}	1.03×10^{-4}	3.00×10^{-6}	0.987
	1	9.39×10^{-4}	7.10×10^{-5}	2.00×10^{-6}	0.640
	2	5.69×10^{-4}	6.30×10^{-5}	1.00×10^{-6}	0.437
	3	4.36×10^{-4}	3.00×10^{-5}	0	0.288
	4	2.79×10^{-4}	1.40×10^{-5}	0	0.198
	5	1.53×10^{-4}	9.00×10^{-6}	0	0.134

Table 5. The number of strand breaks and dose per event for ^{99m}Tc, ^{123}I, ^{111}In, ^{201}Tl, and ^{125}I in the case of (N_2←N) combination.

Radionuclide	Distance (μm)	SSB's difference (N_2←CS)	DSB's difference (N_2←CS)	HDSB's difference (N_2←CS)	Dose difference (N_2←CS)
^{99m}Tc	1-0	18%	22%	29%	19%
	2-0	36%	45%	21%	34%
	3-0	47%	47%	36%	46%
	4-0	52%	49%	57%	55%
	5-0	62%	59%	58%	60%
^{123}I	1-0	25%	33%	7%	25%
	2-0	38%	53%	21%	43%
	3-0	53%	62%	36%	53%
	4-0	61%	63%	29%	63%
	5-0	69%	62%	70%	68%
^{111}In	1-0	11%	16%	20%	26%
	2-0	30%	33%	33%	40%
	3-0	41%	36%	60%	51%
	4-0	49%	54%	67%	59%
	5-0	64%	47%	86%	65%
^{201}Tl	1-0	30%	28%	0%	25%
	2-0	44%	42%	0%	39%
	3-0	53%	55%	0%	52%
	4-0	64%	63%	0%	63%
	5-0	66%	71%	100%	68%
^{125}I	1-0	36%	35%	0%	28%
	2-0	53%	63%	0%	56%
	3-0	67%	79%	0%	68%
	4-0	81%	88%	0%	80%
	5-0	84%	48%	100%	86%

Table 6. Percentage difference in strand breaks and dose per event for ^{99m}Tc, ^{123}I, ^{111}In, ^{201}Tl, and ^{125}I in the case of (N_2←CS) combination at varying distances.

Radionuclide	Distance (μm)	SSB's difference (N_2←Cy)	DSB's difference (N_2←Cy)	HDSB's difference (N_2←Cy)	Dose difference (N_2←Cy)
^{99m}Tc	1-0	16%	18%	30%	19%
	2-0	30%	33%	22%	34%
	3-0	42%	43%	33%	45%
	4-0	51%	40%	50%	53%
	5-0	63%	53%	71%	60%
^{123}I	1-0	20%	16%	20%	25%
	2-0	34%	31%	40%	41%
	3-0	46%	48%	50%	52%
	4-0	58%	60%	71%	62%
	5-0	63%	65%	71%	67%
^{111}In	1-0	14%	31%	17%	15%
	2-0	32%	40%	17%	34%
	3-0	43%	50%	33%	53%
	4-0	48%	50%	50%	55%
	5-0	62%	61%	66%	62%
^{201}Tl	1-0	31%	28%	0%	28%
	2-0	43%	42%	0%	41%
	3-0	51%	64%	0%	54%
	4-0	60%	64%	0%	62%
	5-0	63%	67%	75%	67%
^{125}I	1-0	36%	43%	0%	33%
	2-0	65%	73%	0%	58%
	3-0	71%	88%	0%	72%
	4-0	78%	93%	0%	82%
	5-0	84%	87%	100%	86%

Table 7. Percentage difference in strand breaks and dose per event for ^{99m}Tc, ^{123}I, ^{111}In, ^{201}Tl, and ^{125}I in the case of (N_2←Cy) combination at varying distances.

Radionuclide	Distance (μm)	SSB's difference (N_2←C)	DSB's difference (N_2←C)	HDSB's difference (N_2←C)	Dose difference (N_2←C)
^{99m}Tc	1-0	24%	5%	29%	19%
	2-0	32%	35%	36%	33%
	3-0	41%	37%	44%	44%
	4-0	53%	41%	67%	51%
	5-0	60%	52%	87%	59%
^{123}I	1-0	66%	27%	16%	22%
	2-0	39%	43%	33%	40%
	3-0	45%	54%	67%	50%
	4-0	58%	65%	67%	57%
	5-0	66%	72%	83%	64%
^{111}In	1-0	10%	30%	17%	18%
	2-0	37%	39%	40%	35%
	3-0	50%	52%	60%	45%
	4-0	55%	55%	67%	55%
	5-0	64%	73%	80%	61%
^{201}Tl	1-0	35%	30%	0%	22%
	2-0	44%	54%	0%	37%
	3-0	49%	65%	0%	44%
	4-0	61%	65%	0%	57%
	5-0	61%	76%	100%	62%
^{125}I	1-0	36%	26%	0%	33%
	2-0	60%	64%	0%	57%
	3-0	67%	74%	0%	71%
	4-0	81%	86%	0%	80%
	5-0	88%	78%	100%	86%

Table 8. Percentage difference in strand breaks and dose per event for ^{99m}Tc, ^{123}I, ^{111}In, ^{201}Tl, and ^{125}I in the case of (N_2←C) combination at varying distances.

Radionuclide	Distance (μm)	SSBs difference (N_2←N)	DSBs difference (N_2←N)	HDSB difference (N_2←N)	Dose difference (N_2←N)
^{99m}Tc	1-0	18%	9%	7%	18%
	2-0	34%	36%	21%	29%
	3-0	47%	38%	36%	42%
	4-0	51%	38%	57%	49%
	5-0	63%	60%	69%	56%
^{123}I	1-0	21%	28%	15%	25%
	2-0	33%	47%	17%	40%
	3-0	43%	52%	33%	48%
	4-0	55%	59%	50%	49%
	5-0	62%	61%	78%	64%
^{111}In	1-0	14%	31%	20%	17%
	2-0	30%	36%	25%	32%
	3-0	39%	40%	50%	42%
	4-0	44%	53%	67%	49%
	5-0	58%	72%	75%	58%
^{201}Tl	1-0	28%	28%	0%	21%
	2-0	43%	54%	0%	39%
	3-0	50%	68%	0%	46%
	4-0	60%	64%	0%	56%
	5-0	63%	66%	100%	62%
^{125}I	1-0	42%	32%	0%	35%
	2-0	66%	60%	0%	55%
	3-0	76%	77%	0%	71%
	4-0	81%	85%	0%	80%
	5-0	91%	86%	100%	86%

Table 9. Percentage difference in strand breaks and dose per event for ^{99m}Tc, ^{123}I, ^{111}In, ^{201}Tl, and ^{125}I in the case of (N_2←N) combination at varying distances.

Data availability

All data generated or analysed during this study are included in this published article.

Received: 10 August 2024; Accepted: 29 November 2024
Published online: 03 December 2024

References

1. Asadian, S. et al. β-radiating radionuclides in cancer treatment, novel insight into promising approach. *Pharmacological research, 160*, p. 105070. (2020). https://doi.org/10.1016/j.phrs.2020.105070
2. Idrissou, M. B. et al. Targeted radionuclide therapy using auger electron emitters: the quest for the right vector and the right radionuclide. *Pharmaceutics* **13** (7), 980. https://doi.org/10.3390/pharmaceutics13070980 (2021).
3. Moradi, M. S. & Bidabadi, B. S. Micro-dosimetry calculation of Auger-electron-emitting radionuclides mostly used in nuclear medicine using GEANT4-DNA. *Appl. Radiat. Isot.* **141**, 73–79. https://doi.org/10.1016/j.apradiso.2018.08.019 (2018).
4. Ku, A., Facca, V. J., Cai, Z. & Reilly, R. M. Auger electrons for cancer therapy–a review. *EJNMMI Radiopharmacy Chem.* **4**, 1–36. https://doi.org/10.1186/s41181-019-0075-2 (2019).
5. Rigby, A., Blower, J. E., Blower, P. J., Terry, S. Y. & Abbate, V. Targeted Auger electron-emitter therapy: radiochemical approaches for thallium-201 radiopharmaceuticals. *Nucl. Med. Biol.* **98**, 1–7. https://doi.org/10.1016/j.nucmedbio.2021.03.012 (2021).
6. Beaumont, D. et al. Gallium-67 in the evaluation of sarcoidosis: correlations with serum angiotensin-converting enzyme and bronchoalveolar lavage. *Thorax* **37** (1), 11–18. https://doi.org/10.1136/thx.37.1.11 (1982).
7. Goddu, S. M., Howell, R. W. & Rao, D. V. Cellular dosimetry: absorbed fractions for monoenergetic electron and alpha particle sources and S-values for radionuclides uniformly distributed in different cell compartments. *J. Nuclear Medicine: Official Publication Soc. Nuclear Med.* **35** (2), 303–316 (1994). PMID: 8295004.
8. Steien, S. & Aaseth, J. Thallium-201 as an agent for myocardial imaging studies. *Analyst* **120** (3), 779–781. https://doi.org/10.1039/AN9952000779 (1995).
9. Falzone, N. et al. Absorbed dose evaluation of Auger electron-emitting radionuclides: impact of input decay spectra on dose point kernels and S-values. *Phys. Med. Biol.* **62** (6), 2239. https://doi.org/10.1088/1361-6560/aa5aa4/meta (2017).
10. Salim, R. & Taherparvar, P. Monte Carlo single-cell dosimetry using Geant4-DNA: the effects of cell nucleus displacement and rotation on cellular S values. *Radiat. Environ. Biophys.* **58**, 353–371. https://doi.org/10.1007/s00411-019-00788-z (2019).
11. Ahmadi, P., Zafarghandi, M. S. & Shokri, A. Calculation of direct and indirect damages of Auger electron-emitting radionuclides based on the atomic geometric model: a simulation study using Geant4-DNA toolkit. *Nucl. Instrum. Methods Phys. Res., Sect. B.* **483**, 22–28. https://doi.org/10.1016/j.nimb.2020.08.007 (2020).
12. Whitmore, G. & Schneider, D. Comparative effects of neutrons and X-rays on mammalian cells. *Radiation Effects in Physics, Chemistry and Biology (M. Ebert and A. Howard, eds.)*, pp. 1–17. (1962). https://doi.org/10.2307/3571497
13. Chan, P., Lisco, E., Lisco, H. & Adelstein, S. The radiotoxicity of Iodine-125 in mammalian cells: II. A comparative study on cell survival and cytogenetic responses to125 IUdR, and. *Radiat. Res.* **67** (2), 332–343. https://doi.org/10.2307/3574422 (1976).

14. Michalik, V. Estimation of double-strand break quality based on track-structure calculations. *Radiat. Environ. Biophys.* **32** (3), 251–258. https://doi.org/10.1007/BF01209774 (1993).
15. Jackson, S. P. & Bartek, J. The DNA-damage response in human biology and disease. *Nature* **461** (7267), 1071–1078. https://doi.org/10.1038/nature08467 (2009).
16. Ritter, M. A., Cleaver, J. E. & TOBIAS, C. A. High-LET radiations induce a large proportion of non-rejoining DNA breaks. *Nature* **266** (5603), 653–655. https://doi.org/10.1038/266653a0 (1977).
17. Roots, R., Yang, T. C., Craise, L., Blakely, E. A. & Tobias, C. A. Impaired repair capacity of DNA breaks induced in mammalian cellular DNA by accelerated heavy ions. *Radiat. Res.* **78** (1), 38–49. https://doi.org/10.2307/3575005 (1979).
18. Frankenberg-Schwager, M. & Frankenberg, D. DNA double-strand breaks: their repair and relationship to cell killing in yeast. *Int. J. Radiat. Biol.* **58** (4), 569–575. https://doi.org/10.1080/09553009014551931 (1990).
19. Thompson, L. H. Recognition, signaling, and repair of DNA double-strand breaks produced by ionizing radiation in mammalian cells: the molecular choreography. *Mutat. Research/Reviews Mutat. Res.* **751** (2), 158–246. https://doi.org/10.1016/j.mrrev.2012.06.002 (2012).
20. Almond, P. R. et al. AAPM's TG-51 protocol for clinical reference dosimetry of high-energy photon and electron beams. *Med. Phys.* **26** (9), 1847–1870. https://doi.org/10.1118/1.598691 (1999).
21. Lazarakis, P. et al. Investigation of track structure and condensed history physics models for applications in radiation dosimetry on a micro and nano scale in Geant4. *Biomedical Phys. Eng. Express.* **4** (2), 024001. https://doi.org/10.1088/2057-1976/aaa6aa (2018).
22. Kyriakou, I. et al. Influence of track structure and condensed history physics models of Geant4 to nanoscale electron transport in liquid water. *Physica Med.* **58**, 149–154. https://doi.org/10.1016/j.ejmp.2019.01.001 (2019).
23. Briesmeister, J. F. MCNP-A general Monte Carlo code for neutron and photon transport. *LA-7396-M.* (1986). https://inis.iaea.org/search/search.aspx?orig_q=RN:18044302
24. Titt, U., Bednarz, B. & Paganetti, H. Comparison of MCNPX and Geant4 proton energy deposition predictions for clinical use. *Phys. Med. Biol.* **57** (20), 6381. https://doi.org/10.1088/0031-9155/57/20/6381 (2012).
25. Bernal, M. & Liendo, J. An investigation on the capabilities of the PENELOPE MC code in nanodosimetry. *Med. Phys.* **36** (2), 620–625. https://doi.org/10.1118/1.3056457 (2009).
26. Francis, Z., Villagrasa, C. & Clairand, I. Simulation of DNA damage clustering after proton irradiation using an adapted DBSCAN algorithm. *Comput. Methods Programs Biomed.* **101** (3), 265–270. https://doi.org/10.1016/j.cmpb.2010.12.012 (2011).
27. Allison, J. et al. Recent developments in Geant4. *Nuclear instruments and methods in physics research section A: Accelerators, Spectrometers, Detectors and Associated Equipment, 835*, pp. 186–225. (2016). https://doi.org/10.1016/j.nima.2016.06.125
28. Friedland, W., Dingfelder, M., Kundrát, P. & Jacob, P. Track structures, DNA targets and radiation effects in the biophysical Monte Carlo simulation code PARTRAC. *Mutat. Research/Fundamental Mol. Mech. Mutagen.* **711** (1–2), 28–40. https://doi.org/10.1016/j.mrfmmm.2011.01.003 (2011).
29. Terrissol, M. & Beaudre, A. Simulation of space and time evolution of radiolytic species induced by electrons in water. *Radiat. Prot. Dosimetry*. **31** (1–4), 175–177 (1990).
30. Paretzke, H. Parameters characterizing charged particle track structures. *Loc cit IAEA (1989)*, pp. 72–79. (1989). https://inis.iaea.org/search/search.aspx?orig_q=RN:20064026
31. Agostinelli, S. et al. GEANT4—a simulation toolkit. *Nucl. Instrum. Methods Phys. Res., Sect. A*. **506** (3), 250–303. https://doi.org/10.1016/S0168-9002(03)01368-8 (2003).
32. Incerti, S. et al. The geant4-dna project. *Int. J. Model. Simul. Sci. Comput.* **1** (02), 157–178. https://doi.org/10.1142/S1793962310000122 (2010).
33. Chappuis, F. et al. The general-purpose Geant4 Monte Carlo toolkit and its Geant4-DNA extension to investigate mechanisms underlying the FLASH effect in radiotherapy: Current status and challenges. *Physica Medica*, *110*, p. 102601. (2023). https://doi.org/10.1016/j.ejmp.2023.102601
34. Ding, G. X. Energy Spectra, angular spread, fluence profiles and dose distributions of 6 and 18 MV photon beams: results of Monte Carlo simulations for a Varian 2100EX accelerator. *Phys. Med. Biol.* **47** (7), 1025. https://doi.org/10.1088/0031-9155/47/7/303 (2002).
35. Lindborg, L. & Nikjoo, H. Microdosimetry and radiation quality determinations in radiation protection and radiation therapy. *Radiation protection dosimetry, 143*(2–4), pp. 402–408. (2011). https://doi.org/10.1093/rpd/ncq390
36. Raisali, G., Mirzakhanian, L., Masoudi, S. F. & Semsarha, F. Calculation of DNA strand breaks due to direct and indirect effects of Auger electrons from incorporated 123I and 125I radionuclides using the Geant4 computer code. *Int. J. Radiat. Biol.* **89** (1), 57–64. https://doi.org/10.3109/09553002.2012.715785 (2013).
37. Ganjeh, Z. A., Eslami-Kalantari, M., Loushab, M. E. & Mowlavi, A. A. Investigation of the direct DNA damages irradiated by protons of different energies using geant4-DNA toolkit. *Int. J. Radiation Res.* **18** (4), 809–815. https://doi.org/10.52547/ijrr.18.4.809 (2020).
38. Chen, J., Yun, S., Dong, T., Ren, Z. & Zhang, X. Investigate the radiation-induced damage on an atomistic DNA model by using Geant4-DNA toolkit. *Nucl. Instrum. Methods Phys. Res., Sect. B.* **494**, 59–67. https://doi.org/10.1016/j.nimb.2021.03.010 (2021).
39. Bernal, M. A. et al. An atomistic geometrical model of the B-DNA configuration for DNA–radiation interaction simulations. *Comput. Phys. Commun.* **184** (12), 2840–2847. https://doi.org/10.1016/j.cpc.2013.07.015 (2013).
40. Mahdi, S. M. & Babak, S. B. Dosimetry study on Auger electron-emitting nuclear medicine radioisotopes in micrometer and nanometer scales using Geant4-DNA simulation. *Int. J. Radiat. Biol.* **96** (11), 1452–1465. https://doi.org/10.1080/09553002.2020.1820608 (2020).
41. Adjei, D., Trinh, N. D. & Mostafavi, M. Application of Geant4-DNA for simulating water radiolysis induced by Auger electron-emitting radionuclides. *J. Radiat. Res.* **64** (2), 369–378. https://doi.org/10.1093/jrr/rrac105 (2023).
42. Di Maria, S. et al. Dosimetry assessment of DNA damage by Auger-emitting radionuclides: experimental and Monte Carlo studies. *Radiat. Phys. Chem.* **140**, 278–282. https://doi.org/10.1016/j.radphyschem.2017.01.028 (2017).
43. Howell, R. W. Radiation spectra for Auger-electron emitting radionuclides: report 2 of AAPM nuclear medicine task group 6. *Med. Phys.* **19** (6), 1371–1383. https://doi.org/10.1118/1.596927 (1992).
44. Vaziri, B., Wu, H., Dhawan, A. P., Du, P. & Howell, R. W. MIRD pamphlet 25: MIRDcell V2. 0 software tool for dosimetric analysis of biologic response of multicellular populations. *J. Nucl. Med.* **55** (9), 1557–1564. https://doi.org/10.2967/jnumed.113.131037 (2014).
45. Bardiès, M. & Pihet, P. Dosimetry and microdosimetry of targeted radiotherapy. *Curr. Pharm. Design.* **6** (14), 1469–1502. https://doi.org/10.2174/1381612003399176 (2000).
46. Cornelissen, B., Vallis, A. & K Targeting the nucleus: an overview of Auger-electron radionuclide therapy. *Curr. Drug Discov. Technol.* **7** (4), 263–279 (2010).
47. Salim, R. & Taherparvar, P. Dosimetry assessment of theranostic Auger-emitting radionuclides in a micron-sized multicellular cluster model: a Monte Carlo study using Geant4-DNA simulations. *Appl. Radiat. Isot.* **188**, 110380. https://doi.org/10.1016/j.apradiso.2022.110380 (2022).
48. André, T. et al. Comparison of Geant4-DNA simulation of S-values with other Monte Carlo codes. *Nucl. Instrum. Methods Phys. Res., Sect. B.* **319**, 87–94. https://doi.org/10.1016/j.nimb.2013.11.005 (2014).
49. Goddu, S. M. & Budinger, T. F. MIRD cellular S. values: self-absorbed dose per unit cumulated activity for selected radionuclides and monoenergetic electron and alpha particle emitters incorporated into different cell compartments. *(No Title)*. (1997). https://cir.nii.ac.jp/crid/1130282269679164416

50. Tamborino, G. et al. Modeling early radiation DNA damage occurring during 177Lu-DOTATATE radionuclide therapy. *J. Nucl. Med.* **63** (5), 761–769. https://doi.org/10.2967/jnumed.121.262610 (2022).
51. Alcocer-Ávila, M. E. et al. Radiation doses from 161 tb and 177 Lu in single tumour cells and micrometastases. *EJNMMI Phys.* **pp. 7**, 1–9. https://doi.org/10.1186/s40658-020-00301-2 (2020).
52. Salim, R. & Taherparvar, P. A Monte Carlo study on the effects of a static uniform magnetic field on micro-scale dosimetry of Auger-emitters using Geant4-DNA. *Radiat. Phys. Chem.* **195**, 110063. https://doi.org/10.1016/j.radphyschem.2022.110063 (2022).
53. Ganjeh, Z. A., Eslami-Kalantari, M., Loushab, M. E. & Mowlavi, A. A. Calculation of direct DNA damages by a new approach for carbon ions and protons using Geant4-DNA. *Radiat. Phys. Chem.* **179**, 109249. https://doi.org/10.1016/j.radphyschem.2020.109249 (2021).
54. Zein, S. A. et al. Monte Carlo simulations of electron interactions with the DNA molecule: a complete set of physics models for Geant4-DNA simulation toolkit. *Nucl. Instrum. Methods Phys. Res., Sect. B.* **542**, 51–60. https://doi.org/10.1016/j.nimb.2023.06.004 (2023).
55. Mokari, M., Moeini, H., Soleimani, M. & Fereidouni, E. Calculation and comparison of the direct and indirect DNA damage induced by low energy electrons using default and CPA100 cross section models within Geant4-DNA. *Nucl. Instrum. Methods Phys. Res., Sect. B.* **480**, 56–66. https://doi.org/10.1016/j.nimb.2020.08.011 (2020).

Author contributions

Ali Azizi Ganjgah: Investigation, data curation, writing original draft preparation.Payvand Taherparvar: Conceptualization, methodology, investigation, data curation, writing (review and editing).

Declarations

Competing interests

The authors declare no competing interests.

Research involving human and animal rights

This article does not contain any studies with human participants or animals performed by any of the authors.

Additional information

Correspondence and requests for materials should be addressed to P.T.

Reprints and permissions information is available at www.nature.com/reprints.

Publisher's note Springer Nature remains neutral with regard to jurisdictional claims in published maps and institutional affiliations.

Open Access This article is licensed under a Creative Commons Attribution-NonCommercial-NoDerivatives 4.0 International License, which permits any non-commercial use, sharing, distribution and reproduction in any medium or format, as long as you give appropriate credit to the original author(s) and the source, provide a link to the Creative Commons licence, and indicate if you modified the licensed material. You do not have permission under this licence to share adapted material derived from this article or parts of it. The images or other third party material in this article are included in the article's Creative Commons licence, unless indicated otherwise in a credit line to the material. If material is not included in the article's Creative Commons licence and your intended use is not permitted by statutory regulation or exceeds the permitted use, you will need to obtain permission directly from the copyright holder. To view a copy of this licence, visit http://creativecommons.org/licenses/by-nc-nd/4.0/.

© The Author(s) 2024